A New Boost Converter Based Soft Switched Active Snubber Cell for Power Factor Correction

Naim Suleyman Ting[1*], Yakup Sahin[2], Halil Yetgin[2]

[1]Dept. of Electrical-Electronics Eng., Erzincan Binali Yildirim University, Erzincan, Turkey

nsuleyman@erzincan.edu.tr, Work: +904462240088-43150, Gsm: +905548069071

[2]Dept. of Electrical-Electronics Eng., Bitlis Eren University, Bitlis, Turkey

ysahin@beu.edu.tr, hyetgin@beu.edu.tr

ABSTRACT

This paper introduces a new boost converter based soft switched active snubber cell for power factor correction. In this particular converter, the main switch is turned on by means of zero voltage transition (ZVT) and is turned off with the aid of zero voltage switching (ZVS). The main diode is turned on using ZVS and is turned off using zero current switching (ZCS). In the active snubber cell, the auxiliary switch is turned on by means of ZCS and is turned off using zero current transition (ZCT). No semiconductor device is exposed to the additional voltage stress. In this paper, theoretical analysis of the proposed converter is exhibited and this theoretical analysis is validated both with simulation and experimental study, while operating at 100 kHz switching frequency and 600 W output power. It is demonstrated that the proposed converter has 95.7% efficiency and 0.99 unit power factor at soft switching operation.

Keywords: Power factor correction, hard switching, soft switching, active snubber cell, zero voltage transition

[*]Corresponding Author: nsuleyman@erzincan.edu.tr, Work: +904462240088-43150, Gsm: +905548069071.

This work was fully supported by the Office of Scientific Research Project Coordination of Bitlis Eren University Under the Grant of BEBAP 2017.17.

1. INTRODUCTION

The use of the electrical devices is gradually increasing and more energy is required with the developing technology. However, the available energy resources are being dissipated rapidly. Hence, energy use should be more optimized in terms of its efficiency and cost. It is widely known that national and international constraints and standards are being developed considering power factor and harmonics for energy efficiency and quality. Diverse techniques are employed, for example the so-called Power Factor Correction (PFC) in order to provide the required efficiency and quality. Power factor can be corrected with highly costly passive filter or unduly costly and complex active filter. However, literature on this particular issue mainly focuses on high frequency AC-DC converters based PFC circuits that provide more advantages [1]-[4].

The mean of PFC is to bring near zero reactive power and harmonic currents. These harmonic currents cause undesirable issues such as larger harmonic distortion, poor power factor at AC input voltage and current. For the purpose of PFC, the boost converters are usually benefited in industrial applications [5]-[7]. This is mainly because ease of control and high power density are desired attributes in AC-DC boost converters. To maintain these desired attributes, in the principle an AC-DC boost converter ought to be working with the highest frequency as possible. However, the increase in the frequency induces large amount of switching losses and Electromagnetic Interface (EMI), exorbitant current and voltage stresses, declined efficiency and impractical application scenarios [8]-[11]. To circumvent these problems, the soft switching (SS) techniques are developed and replaced the hard switching (HS) [12]-[25]. Soft switching is realized by active or passive snubber cells that are added to converter. Generally speaking, if SS is achieved by passive snubber cells, this is called as zero current switching (ZCS) at turning-on and zero voltage switching (ZVS) at turning-off. Besides, active snubber cells assisting the development of SS is named as zero voltage

transition (ZVT) at turning-on and zero current transition (ZCT) at turning-off.

The soft switching converters can be categorized as magnetic conductor and non-magnetic according to the structure of snubber cell. The converters containing non-magnetic snubber cell are proposed in [12]-[17]. The basic ZVT converter is presented in [12], which achieves SS at turning-on for the main switch. However, the main switch is turned off using HS in this unique converter. Therefore, the power switching losses cannot be prevented in this converter. In [13], the main switch is switched using SS but, there is an additional current stress across the main switch and there is an additional voltage stress across the auxiliary diode. In [14], the entire semiconductors operate by using SS, where an additional current stress occurs on both the main and the auxiliary switches. Furthermore, an additional voltage stress occurs across the auxiliary diode. In [15], the main switch is turned on using ZVT and is turned off by means of ZVS, whereas the auxiliary switch is turned on and off with the aid of ZCS. However, both switches are exposed to additional current stress and the main switch and diode are also exposed to additional voltage stresses. All semiconductors discussed in [16] operate based on SS techniques and it is advocated that there is no additional stress of current or voltage across the main components. However, the operational conditions of SS are dependent on the amount of load and the performance of SS deteriorates at light loads. In [17], the main switch is turned on by means of ZVT and is turned on with the help of ZVS. The auxiliary switch is turned on and off using ZCS, but high current stress occurs on the auxiliary switch. An active power switch is utilized in [18] rather than the main diode, where SS is achieved at turning-on for all semiconductors. However, the main switch is turned off by HS. Hence, the power loss of the main switch cannot be reduced at turning-off. In [19], SS is achieved for switches but there are extra elements on the main current path. This case leads to the additional conduction losses. In [20], [21], SS strictly depends on duty cycle and SS cannot be achieved under 0.5 duty cycle and an additional current stress is exposed across the

main switch in [21].

In [22], all semiconductors operate using SS techniques, where there is no additional stress of current or voltage across the main elements. The converter having magnetic snubber cell are proposed in [23-25]. A coupled inductor is used in the snubber cell in [23], [24], which ensures ZVT turning-on, but parasitic oscillations arise due to the leakage inductance. In [25], the auxiliary transformer increases the cost of converter and the application of this converter is impractical.

In this treatise, a new boost converter based active snubber cell for PFC is introduced in order to overcome the drawbacks of the above-mentioned soft switched converter. In this particular converter, turning on of the main switch is accomplished using ZVT and of the main diode is achieved by means of ZVS. Similarly, the turning off of the main switch is attained by ZVS and of the main diode is provided by ZCS. Turning on of the auxiliary switch is accomplished by the help of ZCS, while its turning off is attained by ZCT. Noting that semiconductor devices never experience the voltage stress. The converter introduced can function in a wide range of voltage values and reduces EMI. Therefore, the proposed converter outperforms the conventional ZVT boost converter in terms of the overall efficiency. Consequently, this new converter is capable of achieving a less total harmonic distortion and a unit power factor.

2. OPERATIONAL PRINCIPLE AND ANALYSIS

The converter suggested is delineated in Fig. 1, where V_i defines the AC voltage source, V_O describes the output voltage, L_m denotes the filter inductor and C_m stands for the filter capacitor, while D_m represents the main diode, S_m corresponds to the main switch and the body diode is denoted by D_{Sm}, and R_L stands for the output load. In this active snubber cell, S_a stands for the auxiliary switch and D_{Sa} represents its body diode, as well as the auxiliary diode

is expressed by D_a, while C_S denotes the snubber capacitance. Finally, C_r and L_r represent the resonance capacitance and inductance, respectively.

For theoretical analysis, eight operational stages occur in one switching duration. Figure 2 demonstrates the corresponding circuits of these operational stages, whereas the key wave shapes of the converter are portrayed in Figure 3.

Stage 1 [$t_0 < t < t_1$: Fig. 2 (a)]

When $t < t_0$, the voltage of C_S capacitor is identical to the output voltage and the input current flows through to the main diode D_m. At $t = t_0$, a control signal is applied to the gate of S_a. Then, the current of D_m is reduced and the current of S_a is concurrently increased. At $t = t_1$, the current of the main diode declines to zero and the current of S_a arrives at the input current. S_a is turned on and D_m is turned off using ZCS due to serially-connected L_r. Thus, the reverse recovery current of the main diode is significantly reduced. The following equations can be derived for this particular case:

$$i_{Lr}(t) = \frac{V_o}{Z_1}\sin\left(\omega_1(t - t_0)\right) \quad (1)$$

$$v_{Cr}(t) = V_o - V_o\cos\left(\omega_1(t - t_0)\right) \quad (2)$$

$$Z_1 = \sqrt{\frac{L_r}{C_r}} \quad (3)$$

$$\omega_1 = \frac{1}{\sqrt{L_r C_r}} \quad (4)$$

Stage 2 [$t_1 < t < t_2$: Fig. 2 (b)]

At $t = t_1$, a resonance initiates through $C_S - L_r - C_r$. The voltage of C_S is reduced while the current of L_r is increased in sinusoidal form. If the voltage of C_S reaches at zero, then this stage terminates. The equations derived for this stage are as follows:

$$i_{Lr}(t)=\frac{V_1}{Z_2}\sin\left(\omega_2(t-t_1)\right)+I_1\cos\left(\omega_2(t-t_1)\right)-I_1+I_{Lr}(t_1) \quad (5)$$

$$\begin{aligned} v_{Cr}(t)&=\frac{I_{Lm}}{C_r+C_s}(t-t_1)+V_{Cr}(t_1)\\ &-\frac{C_{eq}}{C_r}\left[V_1\cos\left(\omega_2(t-t_1)\right)-I_1Z_2\sin\left(\omega_2(t-t_1)\right)-V_1\right]\end{aligned} \quad (6)$$

$$\begin{aligned} v_{Cs}(t)&=\frac{I_{Lm}}{C_r+C_s}(t-t_1)+V_o\\ &+\frac{C_{eq}}{C_s}\left[V_1\cos\left(\omega_2(t-t_1)\right)-I_1Z_2\sin\left(\omega_2(t-t_1)\right)-V_1\right]\end{aligned} \quad (7)$$

where;

$$I_1=I_{Lr}(t_1)-\frac{C_{eq}}{C_s}I_{Lm} \quad (8)$$

$$V_1=V_o-V_{Cr}(t_1) \quad (9)$$

$$C_{eq}=\frac{C_rC_s}{C_r+C_s} \quad (10)$$

$$Z_2=\sqrt{\frac{L_r}{C_{eq}}} \quad (11)$$

$$\omega_2=\frac{1}{\sqrt{L_rC_{eq}}} \quad (12)$$

Stage 3 [$t_2 < t < t_3$: Fig. 2 (c)]

At $t = t_2$, with the help of ZVS the internal diode of D_{Sm} is turned on and this operation initiates this particular stage. If the body diode D_{Sm} is in the on-state, a gate signal provides the switch S_1, and thus the main switch is turned on using ZVT. Hence, the switching losses during the turning on process are entirely diminished. If V_{Cr} reaches at its affordable level, D_{Sm} is turned off and this stage terminates.

$$i_{Lr}(t) = I_2 \cos\left(\omega_1 (t - t_2)\right) - \frac{V_2}{Z_1} \sin\left(\omega_1 (t - t_2)\right) \quad (13)$$

$$v_{Cr}(t) = I_2 Z_1 \sin\left(\omega_1 (t - t_2)\right) + V_2 \cos\left(\omega_1 (t - t_2)\right) \quad (14)$$

where;

$$I_2 = \sqrt{\frac{L_r I_{Lr}^2 (t_2) - C_r V_2^2}{L_r}} \quad (15)$$

$$V_2 = \frac{I_{Lm}}{C_r}(t_2 - t_1) + \frac{C_s}{C_r} V_o + V_{Cr}(t_1) \quad (16)$$

$$I_{Lr}(t_2) = \frac{\sqrt{V_1^2 + (I_1 Z_2)^2}}{Z_2} + \frac{C_{eq}}{C_s} I_{Lm} \quad (17)$$

Stage 4 [$t_3 < t < t_4$: Fig. 2(d)]

At $t = t_3$, a resonance is commenced between L_r and C_r. The current of L_r is raised immediately upon the voltage of C_r is reduced in sinusoidal form. In this stage, the control signal of S_a is cut off and it is turned off by means of ZCT, while D_{Sa} is in its on-state. Hence, the power losses of S_a are fully eliminated during the turning off process. V_{Cr} falls to zero, at which this stage terminates.

$$i_{Lr}(t) = -\frac{V_{Crpeak}}{Z_1} \sin\left(\omega_1 (t - t_3)\right) \quad (18)$$

$$i_{Lr}(t) = V_{Crpeak} \cos\left(\omega_1 (t - t_3)\right) \quad (19)$$

$$i_{Sm} = I_{Lm} - i_{Lr}(t) \quad (20)$$

where;

$$V_{Crpeak} = \sqrt{\frac{L_r I_2^2 (t_2) + C_r V_2^2 (t_2)}{C_r}} \quad (21)$$

Stage 5 [$t_4 < t < t_5$: Fig. 2 (e)]

This particular stage is on-interval of the classical boost converter and the following equations can be derived for this stage:

$$i_{Lr}(t) = I_{Lrpeak} = \frac{V_{Crpeak}}{Z_1} \tag{22}$$

$$i_{Sm} = I_{Lm} + I_{Lrpeak} \tag{23}$$

Stage 6 [$t_5 < t < t_6$: Fig. 2 (f)]

At $t = t_5$, the gate signal of the main switch is cut off. So, it is turned off by means of ZVS owing to its parallel capacitor of C_S, which is recharged by $I_{Lm} + I_{Lrpeak}$. At $t = t_6$, V_{Cs} reaches at V_O, which terminates this stage.

$$i_{Lr}(t) = i_{Lm} - \left(i_{Lm} + i_{Lrpeak}\right)\cos\left(\omega_1\left(t - t_5\right)\right) \tag{24}$$

Stage 7 [$t_6 < t < t_7$: Fig. 2 (g)]

At $t = t_6$, D_m is turned on by means of ZVS, and so this stage is initiated. The current of L_r inductance is linearly declined during this stage. At $t = t_7$, the current of L_r arrives at zero and this stage terminates. For this stage, following equations can be derived:

$$i_{Lr}(t) = I_{Lr\max} - \frac{V_o}{L_r}(t - t_6) \tag{25}$$

$$i_{Dm} = I_{Lm} + i_{Lr}(t) \tag{26}$$

Stage 8 [$t_7 < t < t_8$: Fig. 2 (h)]

This stage is off-interval of the classical boost converter. At $t = t_8$, it is returned to the beginning of period immediately upon a gate signal is provided for the auxiliary switch. The resulting equation can be obtained in this stage, as follows:

$$i_{Dm} = I_{Lm} \tag{27}$$

3. DESIGN METHODS AND SOFT SWITCHING CONDITIONS

According to the assumptions made in the state-of-the-art literature, following design criteria are outlined in the converter introduced.

a) The choice of snubber capacitor C_r: The duration of ZVT, depicted as $t_{ZVT,}$ is crucial for SS at the time-instant of turning on process. Hence, t_{ZVT} must be larger than t_r, namely rise time of S_m. The relationship between t_{ZVT} and snubber inductance L_r for various snubber capacitance C_r values is illustrated in Fig. 4.

b) The choice of snubber inductor L_r: The reverse recovery duration (t_{rr}) of D_m to select the L_r is important. The current of switch should arrive at the level of input current at most within the duration of $3t_{rr}$ after the auxiliary switch is turned on. Duration t_{rr} of the main diode for the application is chosen as 50 ns. To determine L_r, the following equation can be leveraged:

$$\frac{1}{\omega_1}\sin^{-1}\left(\frac{I_{Lm}Z_1}{V_o}\right)\geq 3t_{rr} \qquad (28)$$

4. SIMULATION APPLICATION AND CONVERTER FEATURES

A. Simulation application

The proposed converter is simulated in PSIM electronics simulation software. The simulated circuit is presented in Fig. 5, while the current and voltage simulation waveforms of S_m, S_a as well as D_m are portrayed in Fig. 6. The simulation waveforms are suitable for both theoretical analysis and experimental results.

B. Converter Features

The fundamental features of the proposed active snubber cell for soft switched power factor correction boost converters can be compiled, as follows:

1- ZVT assists in turning on the main switch, which is turned back off by means of ZVS. The energy recovery of parasitic capacitance of S_m is realized.

2- ZVS aids in turning on the main diode and turned back off with ZCS.

3- The main diode reverse recovery losses are significantly reduced.

4- ZCS helps in turning on the auxiliary switch, which is turned back off with the aid of ZCT.

5- SS can aid in turning on and off the entire elements of semiconductor.

6- The proposed converter can work without hinging on the load current.

7- Main devices are not exposed to additional voltage stress.

8- Auxiliary semiconductor devices never experience voltage stress.

9- The switching period experiences very low transient intervals.

10- Ease of converter handling due to the common ground that switches have.

11- The overall architecture of snubber cell is straightforward.

12- The presented snubber cell could be readily adopted for other basic converters.

13- Additional passive snubber cell is not required for the proposed converter.

14- The proposed converter exhibits a large PF performance.

5. EXPERIMENTAL RESULTS

A prototype of the presented PFC converter is realized operating at 600 W and 100 kHz. It is also verified with the aid of the predicted analysis of the converter. In this experimental study, the value of filter capacitance is set to 470 μF, while the value of the main inductor is set to 1 mH and 2 μH is used for the value of resonant inductor. Additionally, 33 nF is chosen for the value of resonant capacitor and the value of snubber capacitor is set to 3.3 nF. To obtain the gate signals of the switches, the control circuit associated with the UC3854 integrated circuit is devised in the PFC converter. The control circuit is illustrated in Fig. 7. The image of the experimental prototype is provided in Fig. 8.

UC3854A connected converter produces a gate signal for the main switch. The gate signal of the auxiliary switch is gathered by using the gate signal of the main switch through the

instrument of the analog card. Additionally, the semiconductor components utilized in the converter are exhibited in Table 1.

Fig. 9 represents the experimental outcomes of the proposed converter. The gate signals of the switches, the voltage and current wave shapes of the main switch are illustrated in Fig. 9 (a). It can be readily obtained from Fig. 9 (a) that the control signal is applied to the gate of S_m immediately upon the voltage of S_m falls to zero. Hence, S_m is turned on by means of ZVT without the intersection of its current and voltage. Besides, S_m is turned off with the aid of ZVS. Hence, the power losses induced by S_m during the turning on process are significantly diminished and the power losses induced by S_m during the turning off process are considerably reduced. Additionally, the main switch is not exposed to any voltage stress.

The current, the voltage and the control signal wave shapes of S_a are exhibited in Fig. 9 (b). As depicted from Fig. 9 (b), the auxiliary switch is turned on by means of ZCS and is turned off with the help of ZCT. Therefore, switching power losses during the turning on operation is reduced and switching power losses during the process of the turning off is eliminated for the auxiliary switch. Additionally, the auxiliary switch does not experience any voltage stress.

The current, the voltage and the control signal wave shapes of D_m are illustrated in Fig. 9 (c). The main diode is turned on by means of ZVS and is turned off with the help of ZCS. Therefore, its power losses in switching and reverse recovery processes are considerably diminished. Moreover, the main diode is not exposed to any voltage/current stress.

The input voltage and current operating with 220 V input voltage and with 50 Hz frequency are illustrated in Fig. 9 (d). It can be readily obtained from Fig. 9 (d) that the current and voltage wave shape of AC input contains sinusoidal shape. Consequently, the power factor of 0.99 for 220 V AC input voltage at fully load is achieved during the experimental measurements. Additionally, the variance of power factor depends on different line voltage as it is illustrated in Fig. 10.

Fig. 11 compares the efficiency of the proposed converter with the conventional converter topologies. It can be readily observed that the proposed converter is much more efficient than the other converter topologies considering various range of load conditions. For the converter introduced, the efficiency is 91% considering hard switching operation and it is measured about 95.7% considering soft switching operation at 600 W.

6. CONCLUSIONS

In this treatise, a new boost converter based soft switched active snubber cell for PFC is suggested. The introduced converter assists the main switch for turning on using ZVT and turning off using ZVS. Therefore, ZVS is utilized for turning on and ZCS is exploited for turning off for the main diode, while soft switching is implemented for the entire auxiliary semiconductor components. The structure of the introduced converter is straightforward, contains ease of practical application and affordable in cost. Additionally, theoretical findings and simulation results of this research is validated with an experimental prototype considering the parameters of 600 W and 100 kHz. Consequently, the power factor of about 0.99 is achieved for the proposed converter and the efficacy of the converter reaches at 95.7% at nominal output power.

REFERENCES

1. Lee, S.H., Cha, W.J., and Kwon, B.H. “High-efficiency soft-switching AC–DC converter with single-power-conversion method”, *IEEE Trans. Ind. Electron*. 64(6), pp. 4483-4490 (2017).

2. Poorali, B., Adib, E., and Farzanehfard, H. “A single-stage single-switch soft-switching power-factor-correction led driver”, *IEEE Trans. Power Electron*. 32(10), pp. 7932-7940 (2017).

3. Alam, M., Eberle, W., Gautam, D.S., and Botting, C. “A soft-switching bridgeless AC–DC power factor correction converter”, *IEEE Trans. Power Electron*. 32(10), pp. 7716-7726 (2017).

4. Ting, N. S. “A new high power factor ZVT-ZCT AC-DC boost converter”, *J. Electr. Eng. Tech.* 13(4), pp. 1538-1547 (2018).

5. Lee, S.W. and Do, H.L. “Soft-switching two-switch resonant AC–DC converter with high power factor”, *IEEE Trans. Ind. Electron*. 63(4), pp. 2083-2091 (2016).

6. Qian, J., Zhao, Q., and Lee, F.C. “Single-stage single-switch power-factor-correction AC/DC converters with DC-bus voltage feedback for universal line applications”, *IEEE Trans. Power Electron*. 13(6), pp. 1079-1088 (1998).

7. Wang, C.M., Lin, C.H., Lu, C.M., and Li, J.C. “Design and realisation of a zero-voltage transition pulse-width modulation interleaved boost power factor correction converter”, *IET Power Electron*. 8(8), pp. 1542-1551 (2015).

8. Sahin, Y. “A novel soft switching PWM-PFC AC-DC boost converter”, *J. Electr. Eng. Tech.* 13(1), pp. 256-262 (2018).

9. Ting,N.S., Sahin, Y., and Aksoy, I. “Analysis, design, and implementation of a zero-voltage-transition interleaved boost converter”, *J Power Electron.* 17(1), pp. 41-55 (2017).

10. Sahin, Y., Ting, N.S., and Aksoy, I. “A highly efficient ZVT–ZCT PWM boost converter with direct power transfer”, *Electr. Eng.* 100 (2), pp. 1113-1123 (2018).

11. Sahin, Y. and Ting, N.S. “Soft switching passive snubber cell for family of PWM DC–DC converters”, *Electr. Eng.* 100(3), pp. 1785-1796 (2018).

12. Hua, G., Leu, C.S., Jiang, Y. and Lee, F.C.Y. “New zero-voltage transition PWM converters”, *IEEE Trans. Power Electron*. 9(2), pp. 213-219 (1994).

13. Altintas, N. “A new single phase soft switched PFC converter”, *J. Electr. Eng. Tech*. 9(4), pp. 1592-1601 (2014).

14. Tseng, C.J. and Chen, C.L. “New ZVT-PWM converters with active snubbers”, *IEEE Trans. Power Electron*. 13(5), pp. 861-869 (1998).

15. Huang, W. and Moschopoulos, G. “A new family of zero voltage transition PWM converters with dual active auxiliary circuits”, *IEEE Trans. Power Electron*. 21(2), pp. 370-379 (2006).

16. Bodur, H. and Bakan, A.F. “A new ZVT-PWM DC-DC converter”, *IEEE Trans. Power Electron*. 17(1), pp. 40-47 (2002).

17. Wang, C.M. “A new zero-voltage-switching pwm boost rectifier with high power factor and low conduction losses”, *IEEE Trans. Ind. Electron*. 52(2), pp. 427-435 (2005).

18. Park, S. and Choi, S. “Soft-switched CCM boost converters with high voltage gain for high-power applications”, *IEEE Trans. Power Electron*. 25(5), pp. 1211-1217 (2010).

19. Choi, W.Y., Kwon, J.M., Kim, E.H., Lee, J.J., and Kwon, B.H. “Bridgeless boost rectifier with low conduction losses and reduced diode reverse-recovery problems”, *IEEE Trans. Ind. Electron*. 54(2), pp. 769-780 (2007).

20. Ting, N.S., Aksoy, I., and Sahin, Y. “ZVT-PWM DC-DC boost converter with active snubber cell”, *IET Power Electron.* 10(2), pp. 251-260 (2017).

21. Stein, C.M.O. and Hey, H.L. “A True ZCZVT Commutation Cell for PWM Converters”, *IEEE Trans. Power Electron*. 15(1), pp. 185-193 (2000).

22. Lee, D.Y., Lee, B.K., Yoo, S.B. and Hyun, D.S. “An improved full-bridge zero-voltage-transition PWM DC/DC converter with zero-voltage/zero- current switching of the auxiliary switches”, *IEEE Trans. Ind. Appl*. 36(2), pp. 558-566 (2000).

23. Menegaz, P.J.M., Co, M.A., Simonetti, D.S.L. and Vieria, J.L.F. “Improving the operation of ZVT DC-DC converters”, *IEEE 30th Power Electronics Specialist Conference (PESC’99),* pp. 293-297 (1999).

24. Bodur, H. and Bakan, A.F. “A new ZVT-ZCT-PWM DC-DC converter”, *IEEE Trans. Power Electron*. 19(3), pp. 676-684 (2004).

25. Bodur, H. and Yildirmaz, S. “A new ZVT snubber cell for PWM-PFC boost converter”, *IEEE Trans. Ind. Electron*. 64(1), pp. 300-309 (2017).

26. Sahin, Y. and Ting, N. S. “Design and application of a novel snubber cell for soft switched pwm dc–dc converters”, *Sadhana Eng. Sciences*, 44(71), (2019).

List of Captions of Figures and Tables

Fig. 1. The circuit design of the introduced PFC boost converter.

Fig. 2. Corresponding circuit designs of the operational phases in the converter introduced. (a) Stage 1, (b) Stage 2, (c) Stage 3, (d) Stage 4, (e) Stage 5, (f) Stage 6, (g) Stage 7, (h) Stage 8 [26].

Fig. 3. Corresponding key wave shapes for the operational stages in the converter introduced [26].

Fig. 4. The relationship between tZVT and snubber inductance Lr for various values of snubber capacitance Cr.

Fig. 5. Simulated circuit of the proposed converter.

Fig. 6. The simulation waveforms of the voltage and current for Sm, Dm as well as Sa from top to bottom, respectively.

Fig. 7. Control circuit of the proposed converter.

Fig. 8. The image of the experimental prototype.

Fig. 9. Experimental outcomes of the current and voltage wave shapes of (a) Sm, (b) Dm, (c)Sa (200 V/div, 10 A/div, 1 µs/div) and (d) AC input voltage and current wave shapes (100 V/div, 2 A/div, 5 ms/div).

Fig. 10. Power factor for different input voltages and output power.

Fig. 11. Efficiency comparison considering various converter topology.

Table 1. Semiconductor components and specifications utilized for the prototype.

List of Figures and Tables

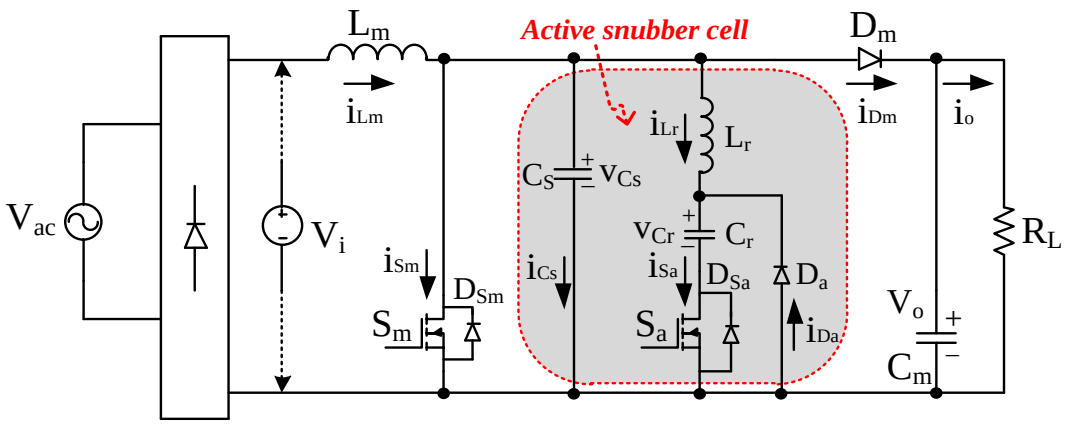

Fig. 1. The circuit design of the introduced PFC boost converter.

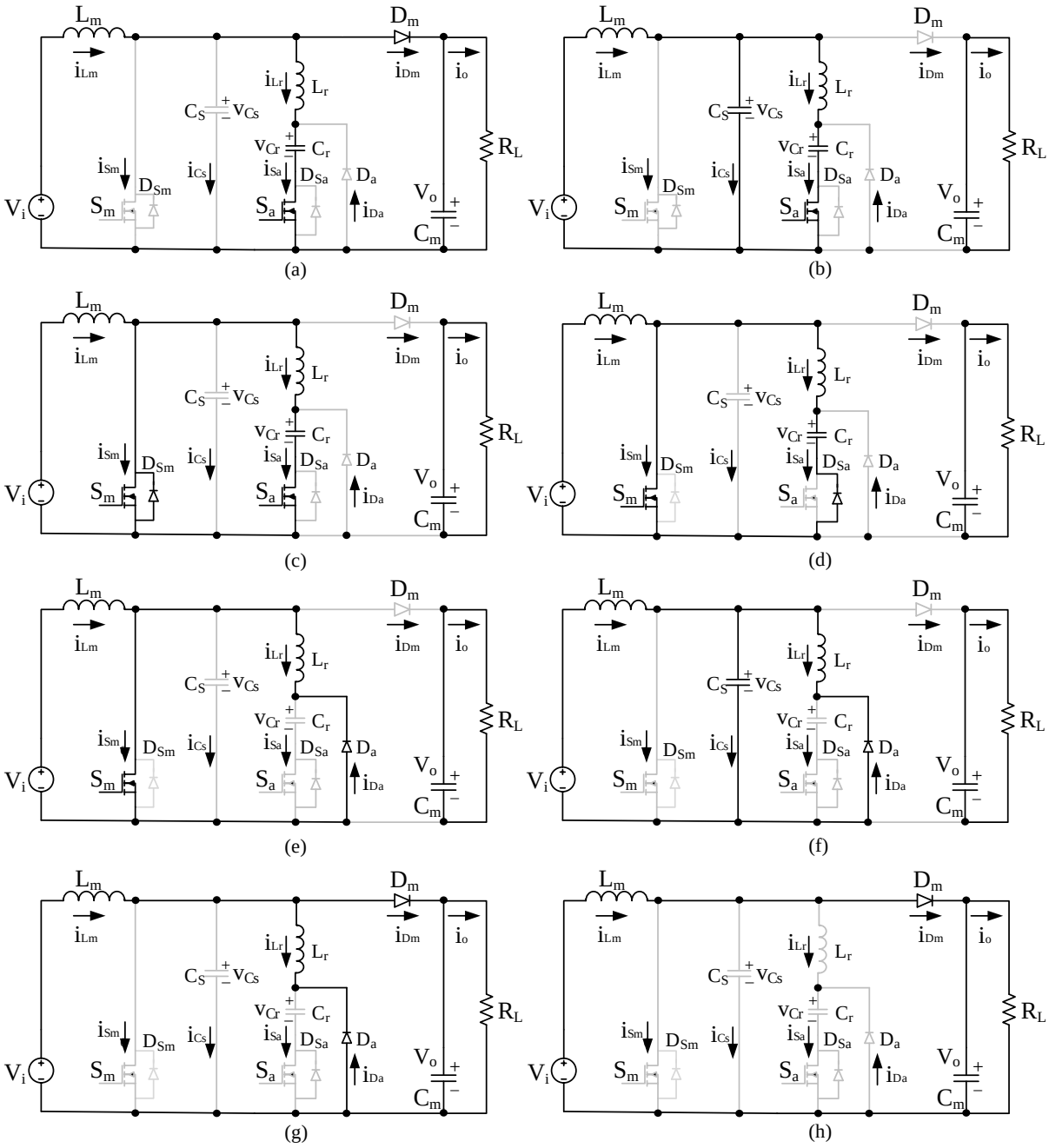

Fig. 2. Corresponding circuit designs of the operational phases in the converter introduced. (a) Stage 1, (b) Stage 2, (c) Stage 3, (d) Stage 4, (e) Stage 5, (f) Stage 6, (g) Stage 7, (h) Stage 8 [26].

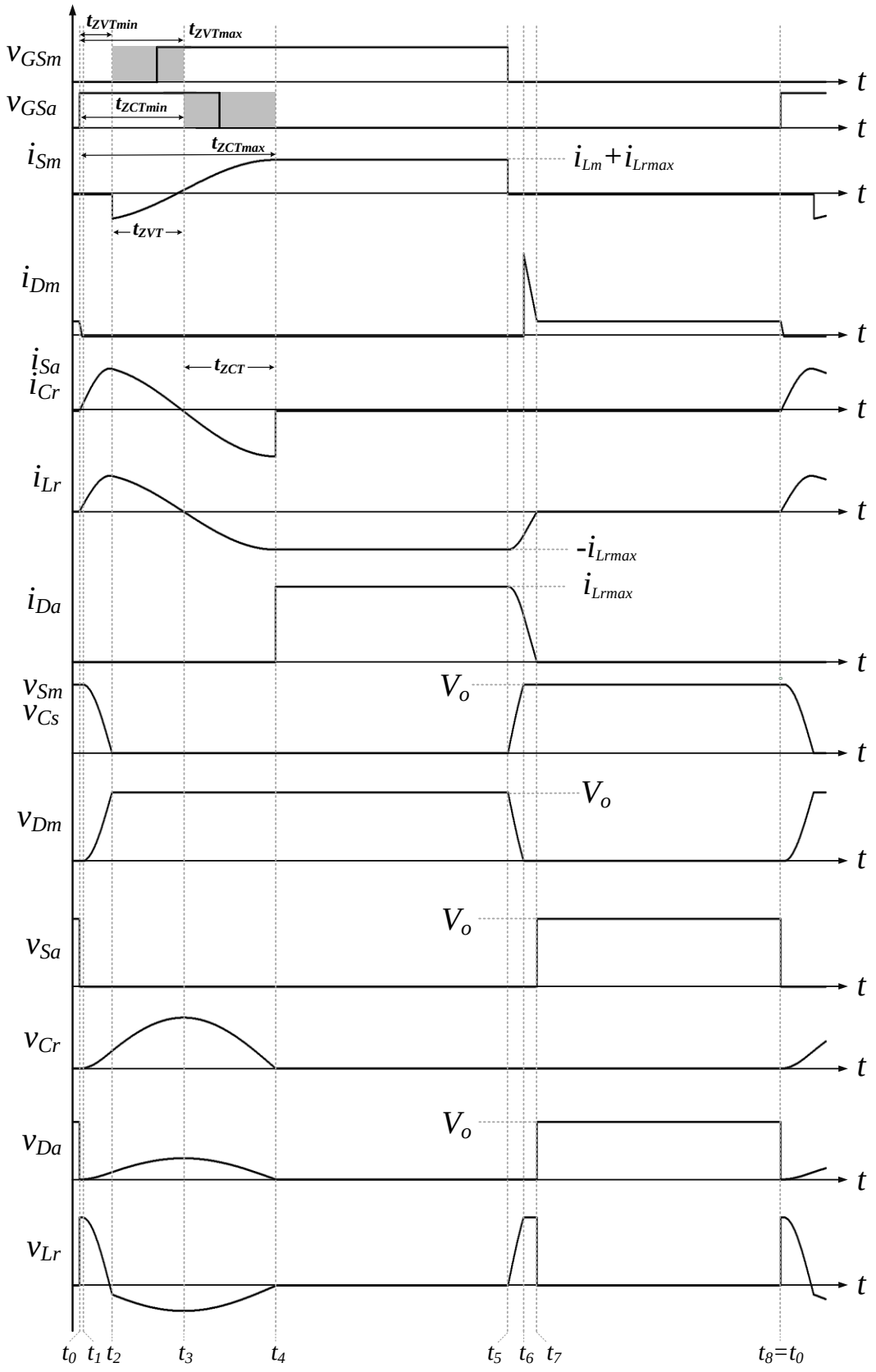

Fig. 3. Corresponding key wave shapes for the operational stages in the converter introduced [26].

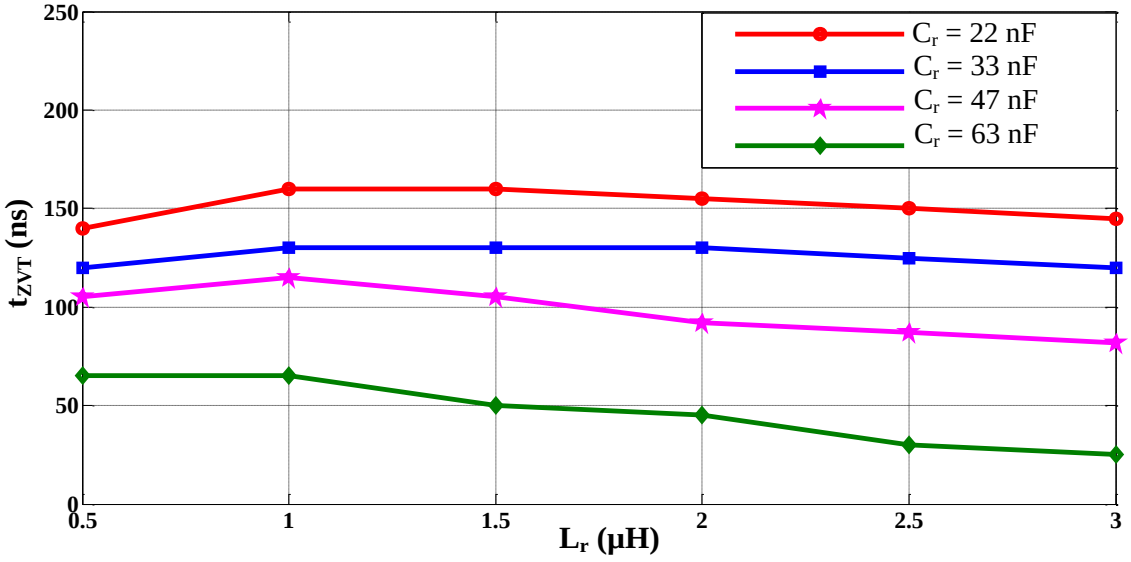

Fig. 4. The relationship between t_{ZVT} and snubber inductance L_r for various values of snubber capacitance C_r.

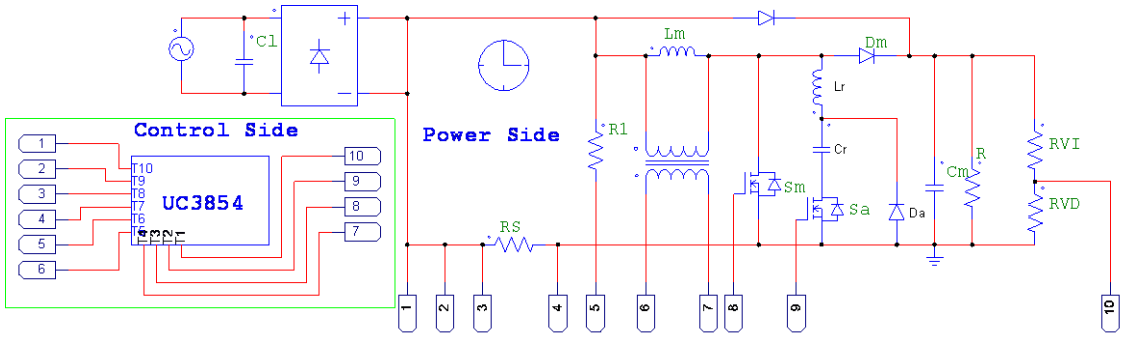

Fig. 5. Simulated circuit of the proposed converter.

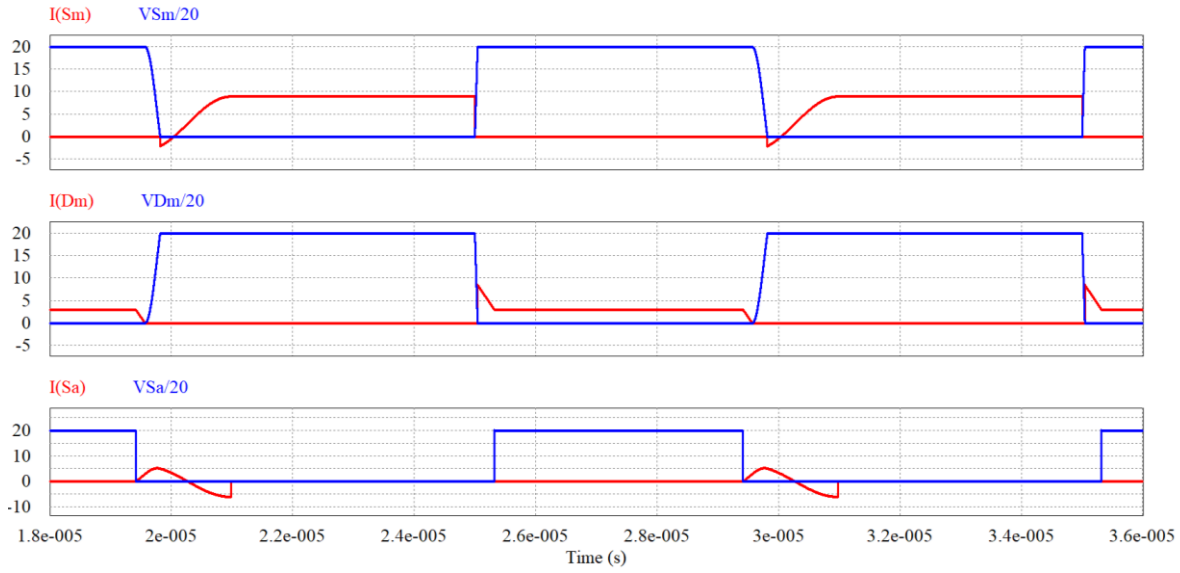

Fig. 6. The simulation waveforms of the voltage and current for S_m, D_m as well as S_a from top to bottom, respectively.

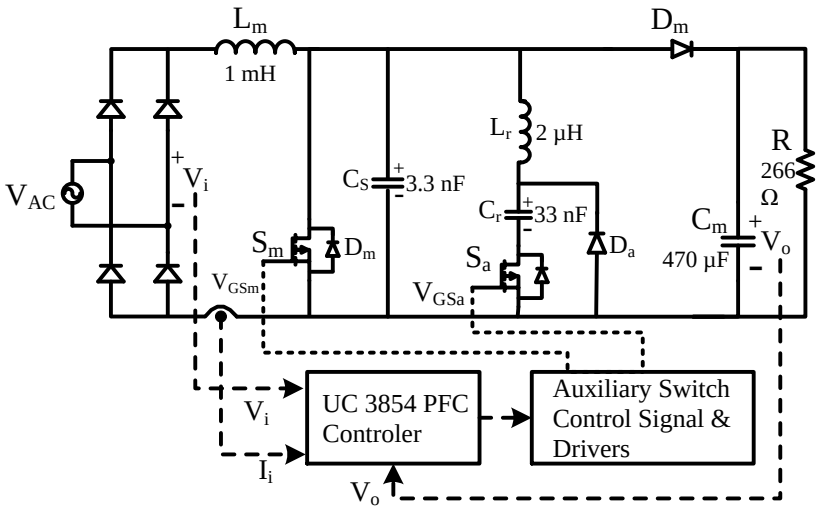

Fig. 7. Control circuit of the proposed converter.

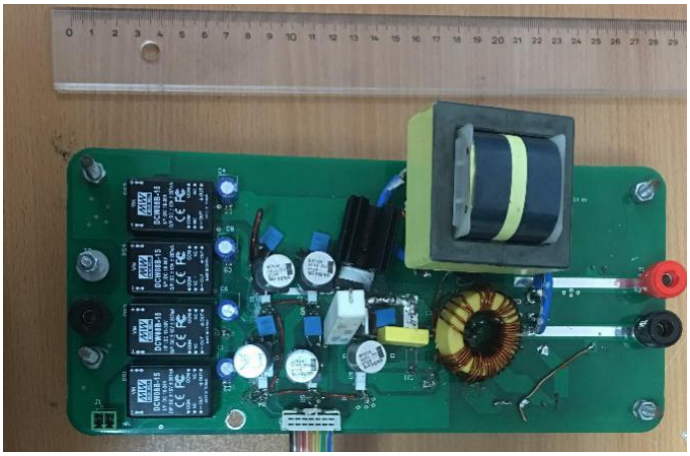

Fig. 8. The image of the experimental prototype.

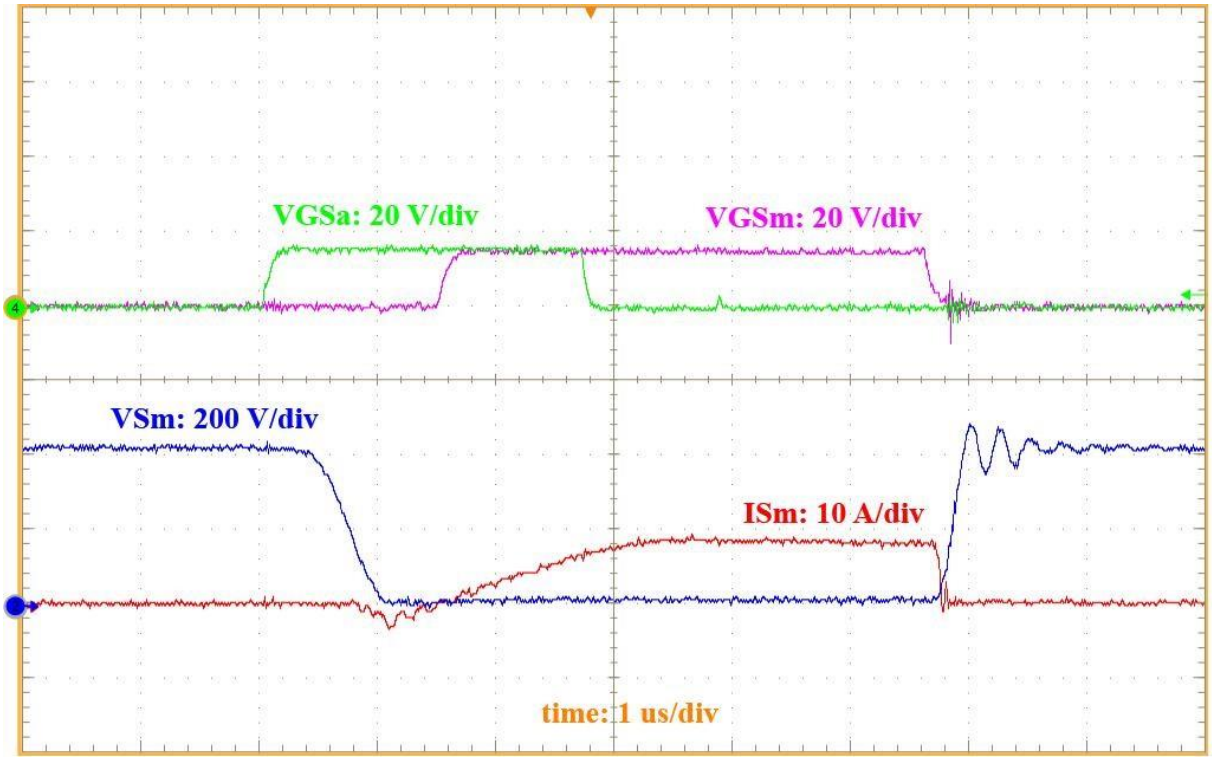
VGSa: 20 V/div
VGSm: 20 V/div
VSm: 200 V/div
ISm: 10 A/div
time: 1 us/div

(a)

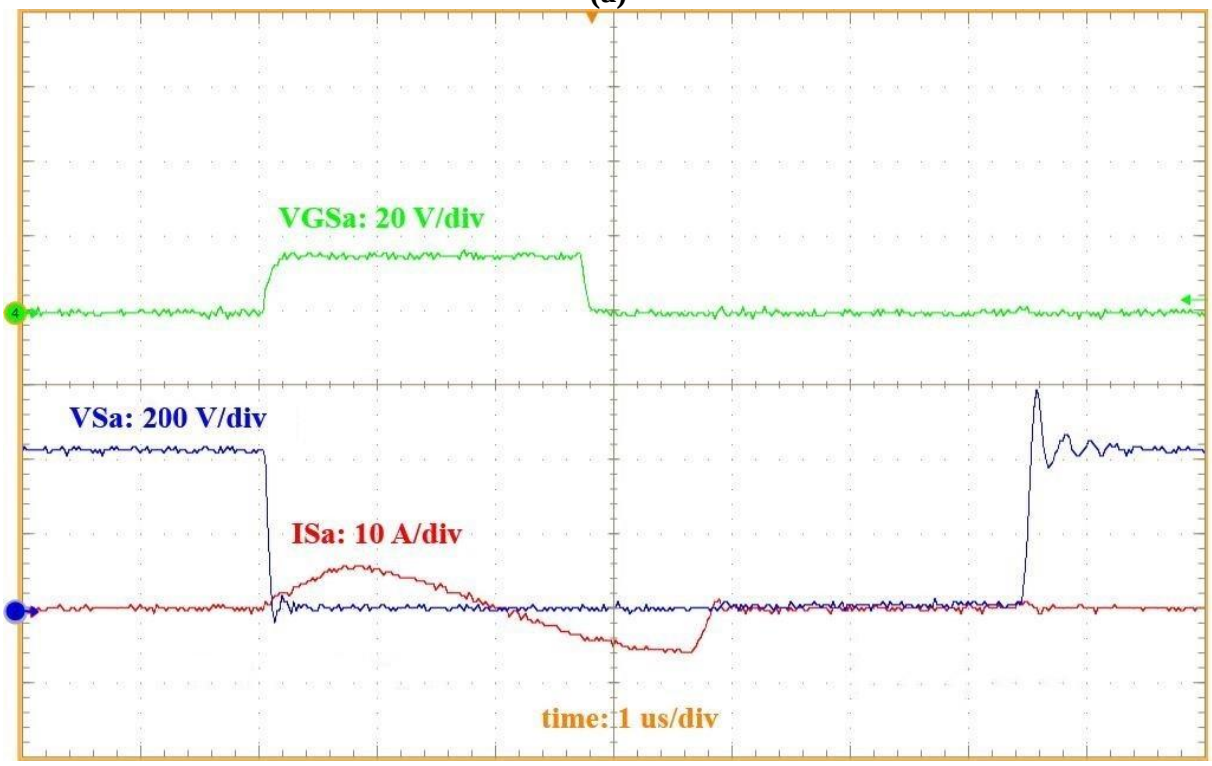
VGSa: 20 V/div
VSa: 200 V/div
ISa: 10 A/div
time: 1 us/div

(b)

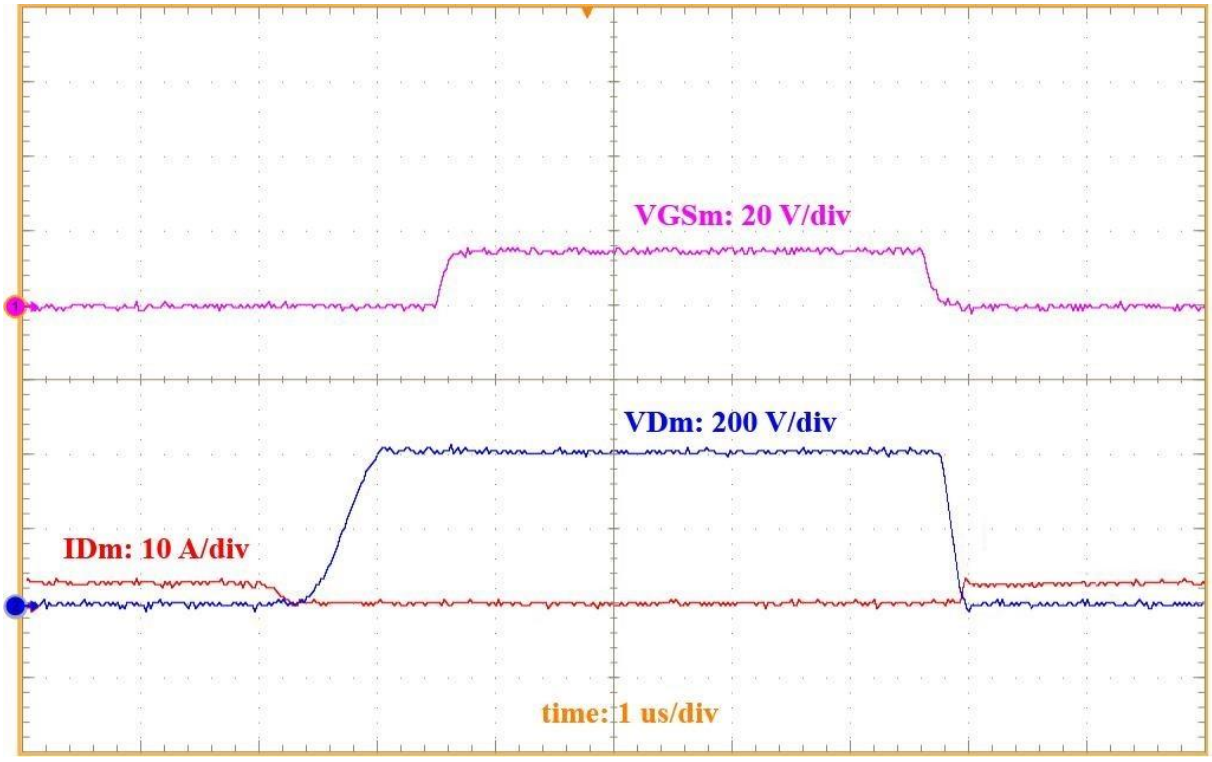
VGSm: 20 V/div
VDm: 200 V/div
IDm: 10 A/div
time: 1 us/div

(c)

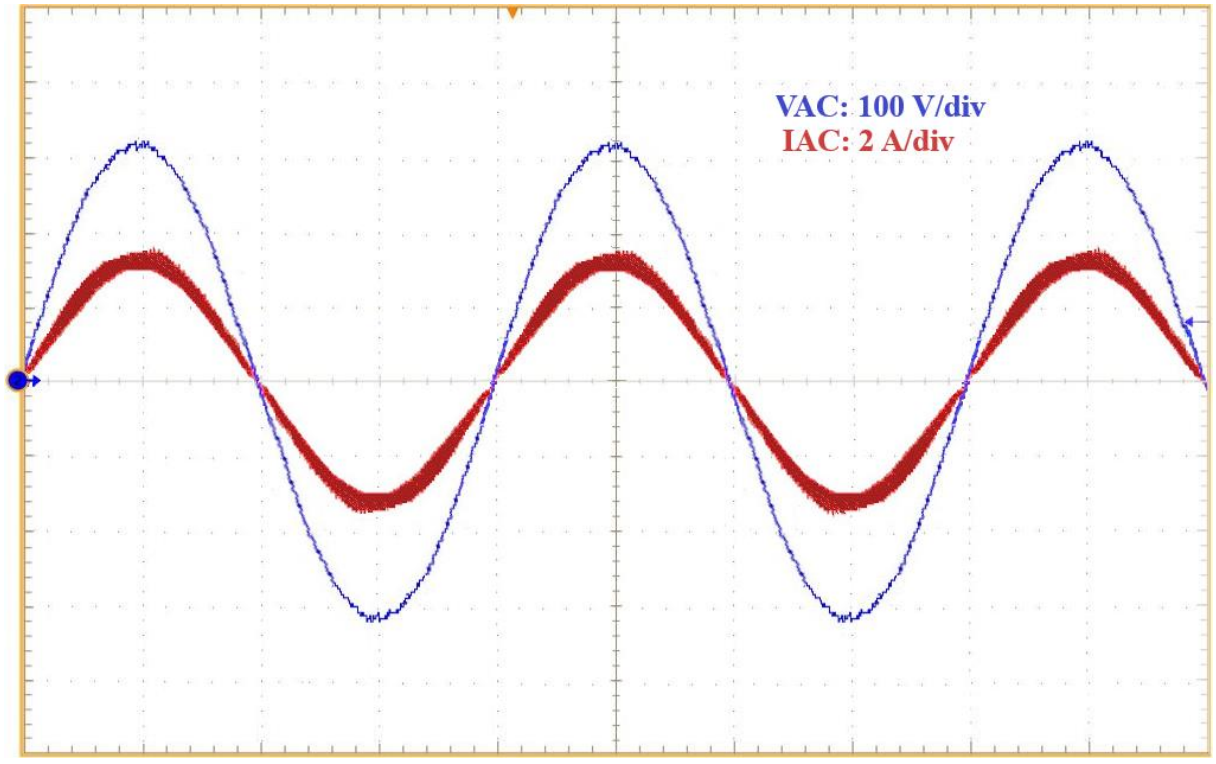
VAC: 100 V/div
IAC: 2 A/div

(d)

Fig. 9. Experimental outcomes of the current and voltage wave shapes of (a) S_m, (b) D_m, (c)S_a (200 V/div, 10 A/div, 1 µs/div) and (d) AC input voltage and current wave shapes (100 V/div, 2 A/div, 5 ms/div).

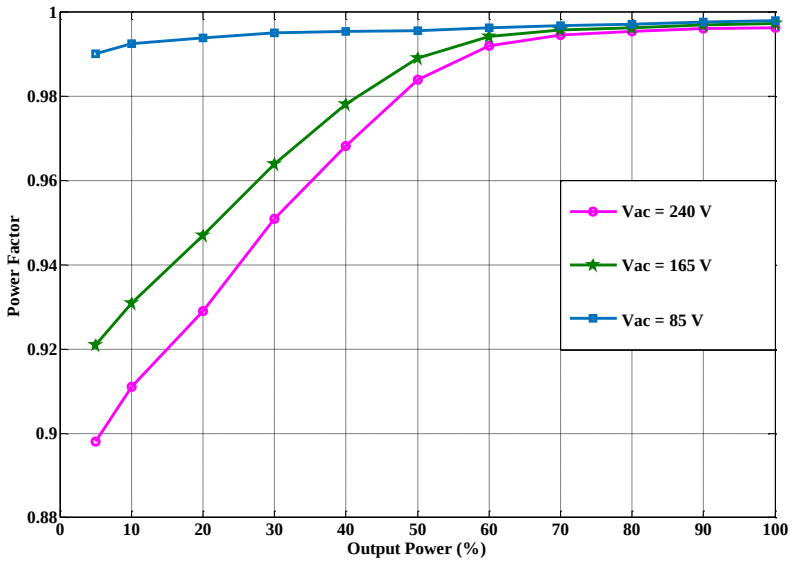

Fig. 10. Power factor for different input voltages and output power.

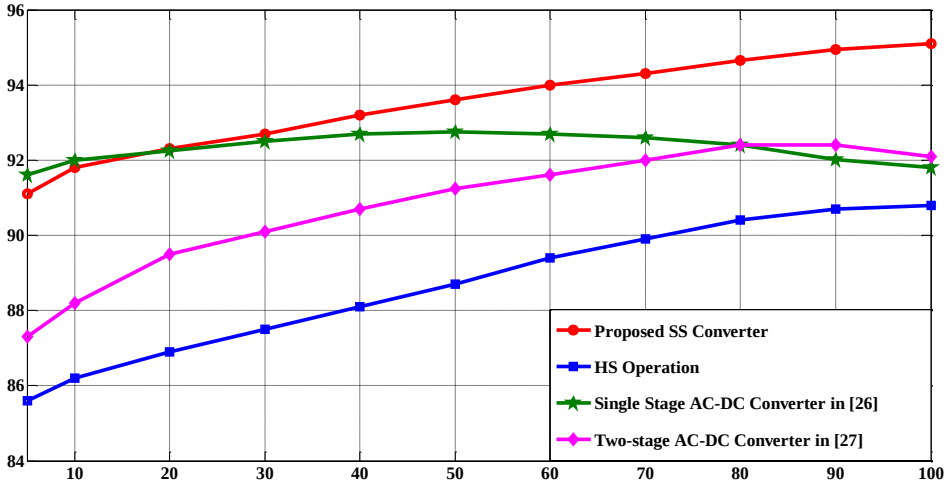

Fig. 11. Efficiency comparison considering various converter topology.

Table 1. Semiconductor components and specifications utilized for the prototype.

Components	Part Number	V [V]	I [A]	t_r [ns]	t_f [ns]	t_{rr} [ns]
S_m	IXFH15N60P	600	15	43	40	250
S_a	FCP190N60E	600	20	14	15	308
D_m	MUR860	600	8	-	-	60
D_a	DESI8-06	600	8	-	-	50

Biographies

Naim Suleyman Ting was born in Erzurum, Turkey in 1988. He received his B.S. degree in Electrical – Electronics Engineering in Erciyes University, Kayseri, Turkey in 2010 and his M.S. and Ph.D. degrees in Electrical Engineering in Yildiz Technical University, Istanbul, Turkey in 2013 and 2016, respectively. He is currently Assistant Professor in the Department of Electrical Electronics Engineering, Erzincan Binali Yildirim University. He has published over 40 journal and conference papers in the area of power electronics. His current research interests include power converters, soft switching, motor control, renewable energy, power factor correction, high frequency power conversion, active and passive snubber cells in power electronics.

Yakup Sahin was born in Adana, Turkey in 1986. He received his B.S. degree from Inonu University, Malatya, Turkey in 2010 and his M.S. and Ph.D. degrees in electrical engineering from Yildiz Technical University, Istanbul, Turkey in 2013 and 2016, respectively. He is currently Assistant Professor in the Department of Electrical Engineering, Bitlis Eren University. His research has been focused on the areas of power factor correction, switching power supplies, high frequency power conversion, and active and passive snubber cells in

power electronics. He has published over 40 journal and conference papers in the area of power electronics.

Halil Yetgin received the B.Eng. degree in computer engineering from Selcuk University, Turkey, in 2008, the M.Sc. degree in wireless communications from the University of Southampton, U.K., in 2010, and the Ph.D. degree in wireless communications from the Next Generation Wireless Research Group, University of Southampton, in 2015. He is currently an Assistant Professor with the Department of Electrical and Electronics Engineering, Bitlis Eren University, Turkey. His research interests include the development of intelligent and industrial communication systems, resource allocation of the future wireless communication networks, UAV communication networks and underwater wireless sensor networks. He was a recipient of the full scholarship granted by the Republic of Turkey, Ministry of National Education.